

Analysis of LLM Vulnerability to GPU Soft Errors: An Instruction-Level Fault Injection Study

Duo Chai, Zizhen Liu, Shuhuai Wang, Songwei Pei, *Member, IEEE*, Cheng Liu, *Senior Member, IEEE*, Huawei Li, *Senior Member, IEEE* and Shangguang Wang, *Senior Member, IEEE*

Abstract—Large language models (LLMs) are highly compute- and memory-intensive, posing significant demands on high- performance GPUs. At the same time, advances in GPU technology driven by shrinking transistor sizes and lower operating voltages have made these devices increasingly susceptible to soft errors. While prior work has examined GPU reliability, most studies have focused on general-purpose applications or conventional neural networks mostly used for vision tasks such as classification and detection. In contrast, systematic analysis of modern large-scale LLMs remains limited, despite their rapid adoption in diverse application scenarios. Given the unique characteristics of LLMs, their resilience to soft errors may differ substantially from earlier models. To bridge this gap, we conduct the first instruction-level fault injection study of LLM inference. Our approach reveals reliability characteristics from multiple perspectives, highlighting the effects of model architecture, parameter scale, and task complexity. These findings provide new insights into LLM reliability and inform the design of more effective fault tolerance mechanisms.

Index Terms—LLM vulnerability analysis, GPU fault injection, GPU soft errors, LLM Reliability.

I. INTRODUCTION

IN recent years, the rapid advancement of large language models (LLMs) such as GPT-4 [1] and DeepSeek [2] has marked a significant milestone in the pursuit of general artificial intelligence. Unlike earlier convolutional neural network models primarily designed for computer vision tasks, LLMs exhibit strong capabilities in natural language understanding, reasoning, and generation, reflecting both broader application scenarios and fundamentally different computational patterns. Executing LLM inference demands substantial computational resources and is widely accelerated by high-performance GPUs, supported by the CUDA programming ecosystem. However, modern GPUs are increasingly vulnerable to transient faults as transistor sizes and operating voltages continue to shrink, reducing design margins. Such faults, which may arise from temperature or voltage fluctuations or from high-energy particle strikes in the environment [3], can corrupt

This paper is supported in part by the National Natural Science Foundation of China (NSFC) under grant No. 62174162 and No.62090024.

Duo Chai, Songwei Pei, Shuhuai Wang and Shangguang Wang are with the School of Computer Science (National Pilot Software Engineering School), Beijing University of Posts and Telecommunications, Beijing 100876, China. Zizhen Liu, Cheng Liu and Huawei Li are with the State Key Lab of Processors, Institute of Computing Technology, Chinese Academy of Sciences, Beijing 100190, China (e-mail: chaiduo@bupt.edu.cn, peisongwei@bupt.edu.cn, liuzizhen@ict.ac.cn, liucheng@ict.ac.cn, wangshuhuai@bupt.edu.cn, liuhuawei@ict.ac.cn, sgwang@bupt.edu.cn), (corresponding authors: Songwei Pei, Cheng Liu).

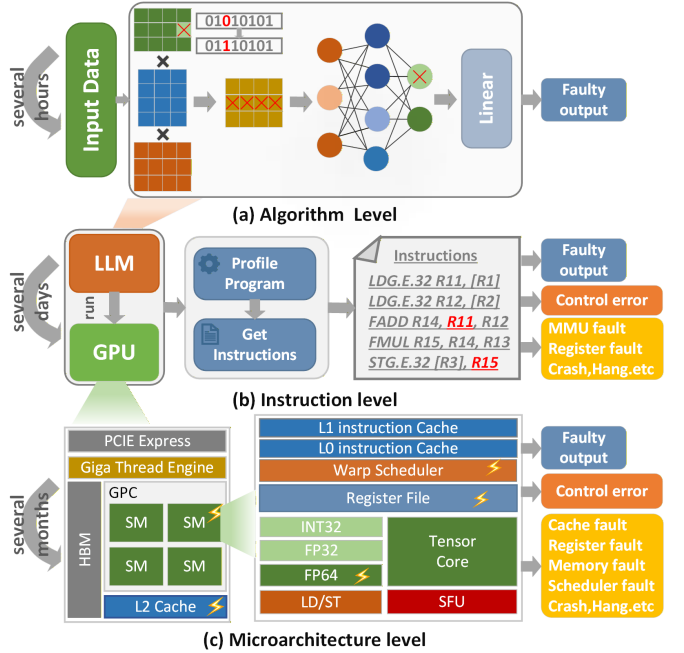


Fig. 1. Typical fault injection approaches at different abstraction levels (1) Algorithm-level fault injection, it injects bit-flip errors to weights and activations at neural network layers. (2) Instruction-level fault injection, it injects bit-flip errors to GPU instructions. (3) Micro-architecture-level fault injection, it injects bit-flip errors at major registers and components of GPU. Essentially, micro-architecture-level fault injection depicts how hardware errors propagate to instructions and algorithms eventually. It is accurate but can be extremely slow. In contrast, algorithm-level fault injection simplifies the error modeling to network operations and ignores low-level details for higher fault simulation speed. Instruction-level fault injection stays between micro-architecture level and algorithm-level fault injection for balanced fault simulation accuracy and speed.

logic or storage states, most commonly manifesting as single-bit flips [4]. Once introduced, these errors may propagate through the computation graph of an LLM, potentially leading to incorrect outputs or system failures. As LLMs are also moving forward to more and more safety-critical domains such as autonomous driving and intelligent healthcare where even minor errors can result in catastrophic consequences, a comprehensive understanding of GPU soft errors in LLMs is urgently demanded.

Significant efforts have been devoted to studying GPU vulnerability to soft errors and mitigating their impact on AI models. However, most existing fault-injection studies for neural networks focus on coarse-grained perturbations, such as weight corruption or layer-wise activation bit-flips as

shown in Figure 1(a). While these approaches are efficient and provide useful insights, they fail to capture the fine-grained computational characteristics of LLMs—such as KV-cache optimizations and operator fusion—which are naturally suited for instruction-level fault injection. Some prior work [5] [6] has investigated the vulnerability of convolutional neural networks (CNNs) to GPU soft errors using instruction-level fault injection, but their conclusions may not generalize to LLMs, which have fundamentally different architectures and tasks. CNNs typically rely on convolutional operators and target vision tasks such as classification and detection, whereas LLMs are based on Transformer architectures and address a broader set of tasks, including reasoning and generation. In addition, the model accuracy metrics also vary substantially. CNN-based vision tasks generally have specific accuracy metrics while LLMs need more complex metrics for evaluation such as Perplexity(PPL) and Exact Match(EM) due to the inherent task complexity. There are also quite some studies [5] [7]–[12] analyzing programs on CPUs or GPUs at the RTL or microarchitecture level using simulators as shown in Figure 1(c). However, such approaches are extremely time-consuming—especially for compute-intensive LLMs—and may not fully reflect the behavior of contemporary GPU architectures.

To achieve both efficient and accurate fault injection evaluation for LLM processing, we adopt NVBitFI [13], [14], an instruction-level fault injection framework (Figure 1(b)), to comprehensively investigate the impact of hardware faults in large language models. We first characterize the overall behavioral distribution of LLM inference systems under diverse hardware fault scenarios and analyze the underlying causes of abnormal behaviors. Building upon this assessment, we perform a systematic study of how instruction types, bit positions, fault models, and network layers influence LLM reliability across a suite of representative tasks, including reasoning and text summarization. Our results demonstrate that task complexity, model scale, and architectural design are key determinants of model vulnerability. To the best of our knowledge, this work is the first to establish a direct connection between transient hardware faults and high-level LLM reliability through instruction-level fault injection, providing new insights into the robustness of large-scale LLM inference systems.

The main contributions of this work are as follows:

- 1) This is the first attempt to systematically assess the reliability of LLMs on GPUs with instruction-level fault injection. Particularly, we analyze the abnormal behaviors of LLM inference in presence of various soft errors and identify their underlying causes.
- 2) We quantify the vulnerability factors of key GPU instruction types and derive an efficient overall vulnerability metric for LLMs based on these factors.
- 3) We investigated a comprehensive vulnerability analysis of LLMs from five perspectives including instruction type, task difficulty, bit position, operator type, and fault layer, revealing how critical architectural parameters of LLMs influence their robustness against soft errors.

II. RELATED WORK

A. GPU Fault Injection

Fault injection is a common method for program reliability evaluation [11] [15]–[18]. While GPU is the mainstream computing engines of deep learning, fault injection on GPU is essential for reliability study of LLMs accordingly. Currently, based on the abstraction levels of the fault injection, GPU fault injection can be roughly classified into two categories: microarchitecture-level fault injection and instruction-level fault injection.

Microarchitecture-level fault injection [7] [12] [19] is typically implemented using the GPGPU-Sim simulator [20], a cycle-accurate and trace-driven simulator that provides a detailed model of GPU microarchitectures. However, the simulation speed can be orders of magnitude slower than realistic GPUs because the low-level simulation involves too many details. This becomes a major barrier in evaluating complex applications such as LLMs which typically require a substantial amount of execution time [21]. In addition, the microarchitectures of the state-of-the-art (SOTA) GPUs are usually unknown to the public making the fault simulation limited to only old GPU architectures which can be distinct to SOTA GPUs.

Instruction-level fault injection, on the other hand, is usually performed using specialized tools such as GPU-Qin [22], LLFI-GPU [23], SASSFI [24], and NVBitFI [13], which inject bit-flip faults into GPU instructions. Since the GPU instruction set is usually available and the fault injection can also be applied on recent off-the-shelf GPU architectures, the simulation speed can be much faster than the microarchitecture-level fault injection tools and enables evaluation of large-scale applications on modern GPU architectures. It has been widely adopted for reliability study on general GPU programs and CNNs [5] [7] [8] [19] [25]–[30] with a lack of work specifically targeting LLMs. Some of these studies attempt to guide software-level fault injection by extracting hardware fault information from the GPU micro-architecture level. Although this approach improves accuracy to some extent, it still suffers from inaccurate hardware information.

In addition to the GPU-specific fault injection methods discussed above, substantial research efforts have been directed toward performing fault injection into neural network models within deep learning frameworks such as PyTorch and TensorFlow. These framework-based fault injection tools typically offer high execution speed, sometimes approaching that of standard deep learning frameworks. However, their error models are generally independent of the underlying computing engines and consequently fail to capture GPU-specific characteristics. As a result, they are primarily limited to investigating computational errors and are mostly employed for algorithm-level fault-tolerant design studies.

B. Reliability Analysis of AI Systems

AI has been increasingly adopted in safety-critical applications such as autonomous driving and robotics, where hardware errors can lead to catastrophic consequences. Consequently, extensive research has been conducted on the reli-

ability of AI models and systems over the past decade [5] [8] [19] [29]–[34]. Existing studies on AI system reliability can be roughly categorized into two directions.

The first category [30], [35]–[37] investigates the impact of hardware faults on AI system behavior and performance metrics, such as accuracy degradation and model vulnerability. These studies aim to understand how hardware errors propagate through neural networks and affect overall model robustness. For example, Roquet et al. [36] systematically evaluated the runtime reliability of large Vision Transformer (ViT) models across two NVIDIA GPU architectures, while He et al. [30] characterized the effects of hardware faults on neural network training processes. Ma et al [35] proposed an SDC detection and mitigation framework based on neuron activation distribution.

The second category [8], [29], [38]–[40] explores design factors that influence AI system reliability—including quantization levels, bit positions, convolution implementations, and layer characteristics—which can provide valuable insights for fault-tolerant AI system design. For instance, Bolchini et al. [8] compared the reliability of neural networks implemented with GEMM, FFT, and Winograd convolution methods. Li et al. [29] conducted an in-depth analysis of how data types, bit positions, layer properties, and data reuse patterns affect error propagation in neural networks. With the emergence of transformer-based architectures, researchers have also begun examining their reliability. Ma et al. [38] analyzed soft error vulnerability in various transformer modules used in ViTs, revealing that certain layers are particularly sensitive to single-bit flips. Similarly, Xie et al. [39] systematically characterized fault tolerance across different layers, bit positions, and architectural components, and proposed a circuit-algorithm co-design fault-tolerance framework.

Despite these advances, most existing reliability studies focus on convolutional neural networks (CNNs), and their conclusions may not directly apply to transformer-based architectures—particularly LLMs, which perform distinct tasks such as reasoning and summarization and rely on different evaluation metrics. Although recent efforts have begun exploring transformer reliability, they generally conduct fault injections at the algorithmic level, which reflects only abstract fault characteristics and fails to capture realistic GPU behaviors. As a result, these approaches are still insufficient for designing fault-tolerant LLMs widely deployed on GPUs. To address these limitations, this work proposes an NVBitFI-based reliability evaluation framework for LLMs that enables comprehensive, instruction-level fault injection on modern GPU devices. This framework facilitates a more accurate and practical analysis of hardware-induced faults, providing insights for developing fault-tolerant LLM systems in real-world GPU environments.

III. LLM VULNERABILITY ANALYSIS ON GPUs

This section mainly investigates the impact of faults on LLM inference systems and evaluates the model vulnerability to bit-flip errors. We conducted comprehensive experiments and spent about 300 GPU hours on the experiments.

A. LLM Reliability Evaluation Framework

Although NVBitFI [13] provides a convenient mechanism for instruction-level fault injection in generic CUDA programs, considerable effort is still required to extend it for LLM reliability evaluation under diverse metrics and fault injection configurations. Figure 2 illustrates the proposed LLM reliability evaluation framework built upon NVBitFI. The framework comprises three main components: fault injection inputs, fault injection for LLMs, and LLM reliability evaluation.

Specifically, the fault injection inputs include the LLM inference program, the model, and the dataset, while users can configure both the fault injection mode and the number of injected faults. To support LLM-specific studies, we extend the primitive bit-flip injection in NVBitFI to higher-level fault injection modes, enabling users to inject faults into specific GPU instructions and, based on execution metadata and results, infer which LLM layer or LLM module these instructions belong to—capabilities essential for investigating LLM vulnerability.

During execution, the framework leverages NVBitFI to intercept GPU kernel operations, collect instruction characteristics, and identify valid fault injection locations. Based on user-defined parameters, it generates a fault injection list and dynamically instruments GPU instructions to flip designated register bits, thereby emulating soft errors.

After fault injection, the framework collects LLM inference outputs, performs statistical analysis of abnormal behaviors (e.g., SDC rate and DUE rate), and computes evaluation metrics such as accuracy, perplexity (PPL), and ROUGE-1. Through this process, the framework enables comprehensive, high-level reliability evaluation of LLM systems.

B. Experiment Setups

All experiments in this study were conducted on a server equipped with an NVIDIA A100 GPU (80 GB), an Intel Xeon Platinum 8358P CPU, and 512 GB of RAM. The software environment consisted of CUDA 12.2, Python 3.12, and NVBit 1.7.5. For model evaluation, we selected three representative LLM architectures—GPT2 [41], Llama3.2 [42], and Qwen3 [43]—with detailed model configurations summarized in Table I. For each architecture, two model scales were evaluated. To comprehensively assess model performance, we adopted benchmark datasets including Lambada [44], PIQA [45], HellaSwag [46], WikiText-2 [47], XSum [48], and GSM8K [49], covering a diverse range of tasks including text generation, mathematical reasoning, and language modeling.

C. Abnormal behavior analysis

Unlike reliability studies based on algorithm-level fault injection, which primarily target data errors during computation, instruction-level fault injection enables a more comprehensive investigation of abnormal behaviors induced by hardware errors. Therefore, we begin with an analysis of the abnormal behaviors observed in the LLM system. In general, the consequences of LLMs under hardware faults can be categorized into three types: detected unrecoverable errors (DUE), silent data corruption (SDC), and masked errors. DUE

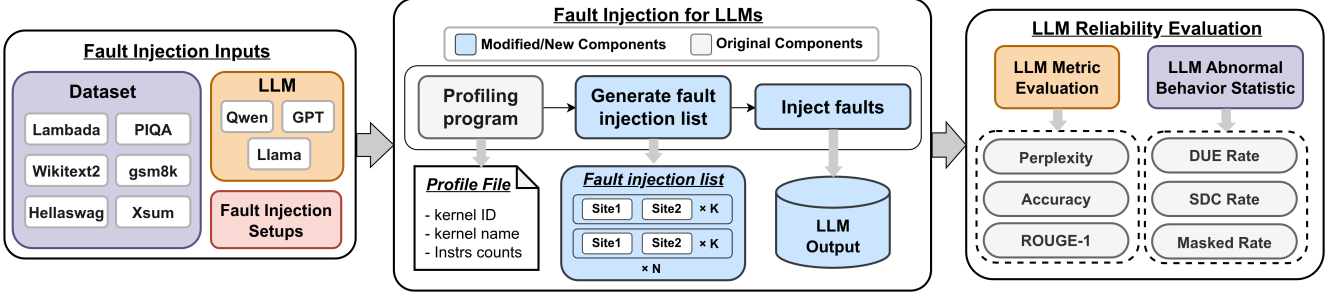


Fig. 2. The Proposed LLM Reliability Evaluation Framework based on NVBitFI.

TABLE I
DETAILED PARAMETER DESCRIPTION OF THE SELECTED MODELS

Model	P	L	HS	AH	VS	CL
GPT2	124M	12	768	12	50257	1k
GPT2-large	774M	36	1280	20	50257	1k
Llama3.2-1B	1.23B	16	2048	32	128256	128k
Llama3.2-3B	3.21B	28	3072	24	128256	128k
Qwen3-0.6B	0.59B	28	1024	16	151936	40k
Qwen3-1.7B	1.72B	28	2048	16	151936	40k

Notes: P=Parameters, L=Layers, HS=Hidden size, AH=Attention heads, VS=Vocabulary Size, CL=Context Length. 1k=1024, 1M=1 Million, 1B=1 Billion

typically refers to system-level failures such as crashes or hangs. SDC denotes cases where the system produces incorrect outputs while appearing to operate normally. Masked refers to scenarios in which the injected faults are effectively masked, and the computation results remain correct.

As shown in Figure 3, abnormal behaviors vary substantially as the number of injected faults increases. Overall, the rate of abnormal outcomes rises sharply, mainly due to surges in both DUE and SDC. Specifically, the abnormal rates of the evaluated LLMs grow from roughly 15%, 25%, and 30% to over 75% as the number of injected faults increases from 1 to 8, indicating severe degradation in inference correctness as bit-flip errors accumulate. Similar to conventional applications, most errors in LLMs can be masked when only a single bit flip is injected. However, the abnormal behaviors of LLMs also exhibit several distinctive characteristics, discussed as follows:

1) *Model scale effect*: For the same LLM architecture, larger models exhibit a higher proportion of masked errors and tend to be more reliable than smaller ones. A plausible explanation is that larger models contain more parameters and activation units, which reduces the fraction of parameters affected by faults. This, in turn, lowers the probability of inference failures caused by a single error.

2) *Architectural sensitivity*: The underlying architecture of an LLM significantly influences its vulnerability to hardware faults. Notably, GPT2 is slightly more resilient than Qwen3-1.7B, even though GPT2 is much smaller in scale. This can be attributed to the normalization strategy: GPT2 employs LayerNorm both before and after each sublayer, which normalizes by standard deviation and subtracts the mean, effectively suppressing large deviations. In contrast, Qwen3 adopts RMSNorm, which normalizes only by the root mean

square without mean subtraction. As a result, RMSNorm is less effective at mitigating single-point deviations, allowing soft errors to persist and amplify through the forward pass.

3) *Dynamic relationship between DUE and SDC*: As the number of injected faults increases, the proportion of DUE grows rapidly, whereas SDC increases much more slowly. This is likely because many potential SDCs are preempted by DUEs that terminate execution prematurely. Only completed inferences that produce incorrect results are counted as SDCs. With more injected faults, an increasing number of inferences are aborted midway due to exceptions, preventing them from being classified as SDCs. This explains the observed dynamic where DUE grows quickly while SDC increases slowly.

With this framework, we can further derive the Model Vulnerability Factor (MVF), as illustrated in Figure 4, which quantifies the likelihood that a transient hardware fault (such as a soft error) leads to a user-visible failure in an LLM's output, following the definition of the traditional program vulnerability factor. Essentially, the MVF is calculated as the sum of the SDC rate and the DUE rate, as illustrated in Figure 3. Compared to conventional programs, the MVF of LLMs tends to be significantly higher, primarily due to their elevated DUE rate.

D. The Causes of DUEs

Based on the experimental results shown in Figure 3, we observe that even when only a single bit flip is injected, the proportion of detected but uncorrectable errors (DUE) remains substantial and is significantly higher than that of conventional applications. Moreover, as the number of injected faults increases, DUE gradually becomes the dominant type of anomalous behavior. To further investigate the root causes of DUE, we perform 3,000 fault injection experiments for each model and analyze system logs to categorize the causes of DUE, as summarized in Figure 4.

The experimental results show that the causes of DUE can be broadly grouped into eight categories: address out-of-bounds, MMU faults, register out-of-bounds, misaligned addresses, invalid instruction operands, PCIe bus errors, thermal violations, and other causes. These categories are denoted as E1–E8, respectively. Among them, E1, E3, E4, and E5 are essentially instruction-level errors, most of which are related to illegal memory accesses; E2 and E6 correspond to hardware-level failures; and E7 is triggered by thermal violations,

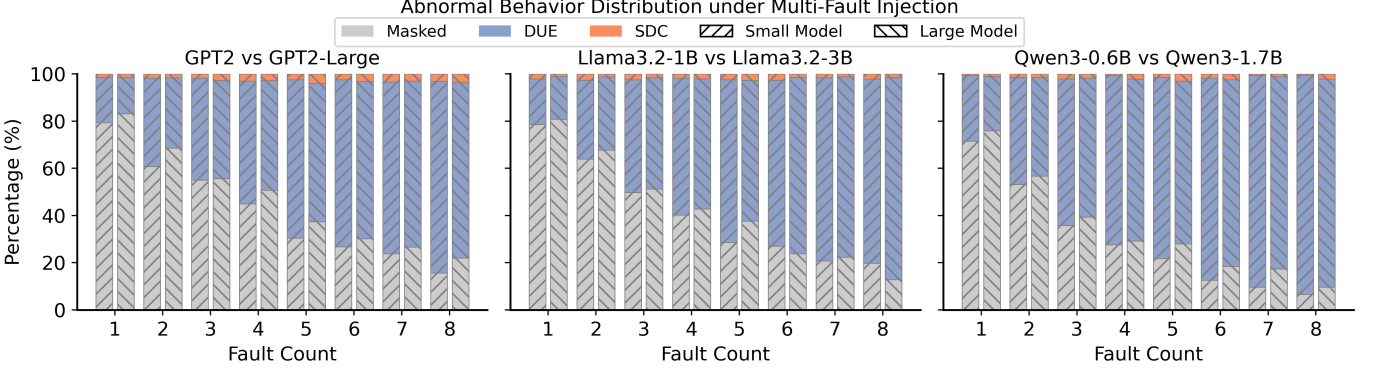


Fig. 3. GPU behavior distribution of LLMs inference system under Multi-Fault scenarios.

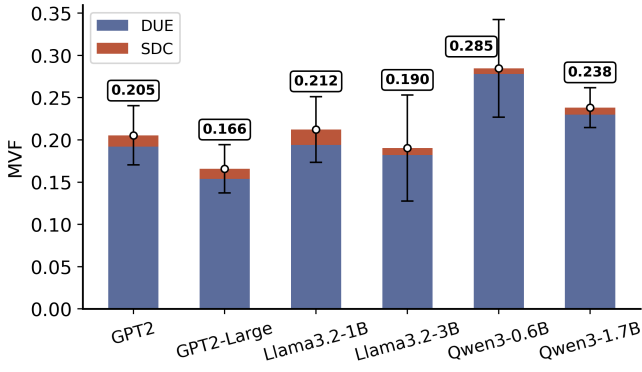


Fig. 4. Model Vulnerability Factors (MVF) of different LLMs. The error bars represent the standard deviation of the MVF over multiple experiments.

indicating that overheating is also a non-negligible source of DUE. The remaining cases that cannot be unambiguously identified from system logs are grouped into the “other” category. We observe that over 90% of DUE events are ultimately attributed to illegal memory accesses induced by bit flips. This is largely because LLM kernels involve intensive memory operations, and address fields occupy a substantial fraction of the instruction bit-width. Consequently, the probability of address corruption is higher than in conventional programs.

In our fault injection experiments, we find that GPT2 is more prone to E1 errors, whereas Qwen and Llama more frequently trigger E3. This discrepancy stems from differences in model architectures and kernel implementations. GPT2 relies heavily on frequent off-chip memory accesses and address computations, and its kernels contain numerous explicit memory load and offset operations; as a result, bit flips are more likely to cause address out-of-bounds errors. By contrast, Qwen and Llama employ highly fused operators such as FlashAttention and RMSNorm, which are compute-intensive and incur high register pressure, with a large portion of intermediate results residing in registers. Under these conditions, bit flips are more likely to corrupt register indices or register-resident data, thereby leading to register out-of-bounds errors.

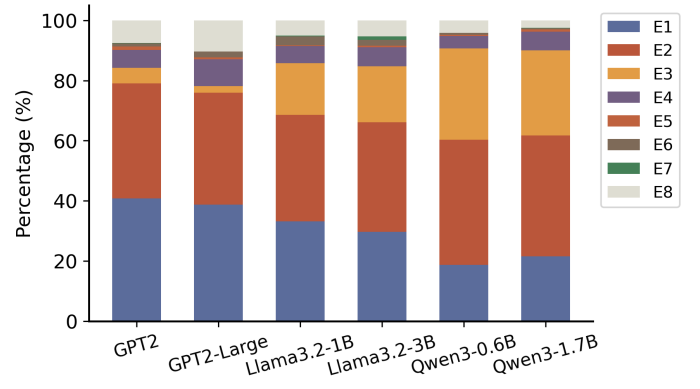


Fig. 5. E1-E8 represent the following types of fault. E1: Out Of Range Address, E2: MMU Fault, E3: Out Of Range Register, E4: Misaligned Address, E5: Illegal Instruction Parameter, E6: PCIe Bus Error, E7: temperature above threshold, E8: others.

E. The Causes of SDCs

In this experiment, we injected 3,000 bit-flip faults into each LLM and observed exactly 200 instances of SDC. Through a detailed analysis of the corresponding SASS code for each SDC, we identified two primary causes: (1) numerical errors, particularly those that lead to large deviations, and (2) address errors that result in incorrect memory loading or writing. Among the observed cases, 178 were attributed to numerical errors, while the remaining 22 were due to address errors.

Large numerical deviations represent a major source of SDCs. A representative example is shown in **List 1**. The registers marked in green contain correct data, while the register highlighted with a red box indicates where the bit flip occurred. Register **R13** was expected to be computed by the **MUFU.RCP** instruction as the reciprocal of **R24**, yielding a theoretical value less than 1. However, in the instruction **0x290 FFMA R13, R13, R12, R13**, a single bit flip altered **R13**’s floating-point value from **0x3e4ccccd** to **0x7e4ccccd**, causing the numerical result to jump from approximately 0.2 to about 3.4×10^{38} . This abnormal value subsequently propagated through later computations—for instance, in the instruction **0x2d0 FFMA R14, R16, R13, R14**, the value of **R14** was excessively amplified, diverging completely from its expected range. As the fault continued to

propagate, it ultimately resulted in an SDC.

An example of a typical address error leading to SDC is shown in **List 2**. In the instruction `0x1010 IMAD R2, R2, c[0xecc], R19`, a bit flip occurred in **R2**, corrupting the address value it stored. This erroneous address was subsequently used for further address calculations in `0x1030 IMAD.WIDE.U32 R2, R2, R3, c[0x160]`, and eventually in `0x1070 STG.E.U16 [R2.64], R17`. Since **R2** already contained a corrupted address, the correct value of **R17** was written to an incorrect memory location, resulting in an SDC. In more severe cases, when the corrupted address becomes illegal, such as in out-of-bounds or misaligned memory accesses, it can lead to program crashes.

1 **Case 1:**

2 `0x0d0 MOV R16,RZ;`

3 `0x160 FADD R24,R16,1;`

4 `0x210 MOV R13,R24;`

5 `0x220 MOV R12,0x240;`

6 `0x230 CALL.REL.NOINC 0x2210;`

7 `0x240 MOV R13,R18;`

8 `0x250 BRA 0x2a0;`

9 `0x260 MUFU.RCP R13,R24;`

10 `0x270 FFMA R12,R24,R13,-1;`

11 `0x280 FADD.FTZ R12,-R12,-RZ;`

12 `0x290 FFMA R13,R13,R12,R13;`

13 `0x2b0 FADD R25,R24,1;`

14 `0x2c0 HADD2.F32 R19,-RZ,R8.H1_H1;`

15 `0x2d0 FFMA R14,R16,R13, R14;`

16 `.....`

Listing 1. Numerical errors leading to SDC. Green represents correct data, red represents data with error propagation, and the registers marked with red boxes represent registers where bit reversals occurs.

1 **Case 2:**

2 `0x0ff0 IMAD.U32 R2,RZ,RZ,UR6;`

3 `0x1000 IMAD R19,R18,c[0xeb8],R19;`

4 `0x1010 IMAD R2,R2,c[0xecc],R19;`

5 `0x1020 IMAD.MOV.U32 R19,RZ,RZ,c[0xc];`

6 `0x1030 IMAD.WIDE.U32 R2,R2,R3,c[0xd];`

7 `0x1070 STG.E.U16 [R2.64],R17;`

8 `.....`

Listing 2. Address errors causing SDC. Green represents correct data, red represents data with error propagation, and the registers marked with red boxes represent registers where bit reversals occurs.

IV. ANALYSIS OF FACTORS AFFECTING LLM VULNERABILITY

In this section, we conduct a multi-dimensional vulnerability analysis of LLMs, aiming to examine all potential factors that may affect their resilience. Specifically, we perform a detailed investigation from five perspectives: instruction types, task variations, bit positions, operator types, and layer variations.

The experiments in total consume approximately 1,750 GPU hours.

A. Instruction Types

1) *Analysis of experimental results:* Since we conduct the fault injection at instruction level, we investigate LLM vulnerability from the perspective of instructions naturally. First of all, we analyze the instruction distribution of the different LLMs. As shown in Figure 6, the computation instructions account for the largest proportion of LLM, averaging 71.8%, primarily consisting of FADD, HMMA, IMAD, and IADD3. This dominance is obvious, since LLM inherently involves intensive data computation. Data transfer instructions such as move and load/store account for an average of 5.8%. Second, we further explore the instruction vulnerability factors (IVF) with fault injection experiments and the result is presented in Figure 7. Note that IVF represents the likelihood of an instruction that results in faulty outputs of the target LLM in the presence of bit-flip errors.

It can be observed that the instructions exhibit distinct vulnerability factors. Some of the instructions such as FADD, FMUL, HMMA, LDG are more resilient while some of the instructions such as SHF, LOP3, and LEA are much more vulnerable. One of the major reasons is that LOP3 and LEA are often associated with address computations, where an error in the address calculation chain can easily lead to illegal memory access or incorrect data retrieval, posing a serious threat to system reliability. Fortunately, the highly vulnerable instructions such as SHF, LEA, and LOP3 generally do not appear frequently in LLMs according to Figure 6. Meanwhile, the most frequently used instructions including FADD and HMMA are less vulnerable. Hence, the protection overhead of these instructions becomes moderate eventually. Nevertheless, IMAD and IADD3 exhibits moderate IVF and takes up non-trivial proportion of the total instructions of LLMs. As a result, they may induce considerable protection overhead.

In addition, we observe that integer computation instructions primarily lead to DUEs across all models, as they are heavily involved in address calculations. Floating-point instructions, on the other hand, are more likely to cause SDCs, accounting for 59% of all SDCs — a trend particularly evident in the GPT2 and Llama3.2 family. This suggests that focusing on floating-point computation instructions is key to mitigating the majority of SDCs.

Another observation is that, across different models, the IVF of the same instruction type is generally consistent, except for FFMA, HADD2, HMMA, LDS, and LDG. The discrepancies in these specific instructions may stem from differences in data paths and compiler optimization strategies among models. For example, certain floating-point and memory-related instructions may have different execution orders or data access patterns in different models, which leads to variations in their IVF values. In addition, we also notice that IVF of the same LLM architecture is highly consistent across most of the instruction types, which indicates that LLM architecture also poses moderate influence on the instruction vulnerability.

Insight #1: LLM instruction-level vulnerability is primarily governed by instruction type rather than directly determined

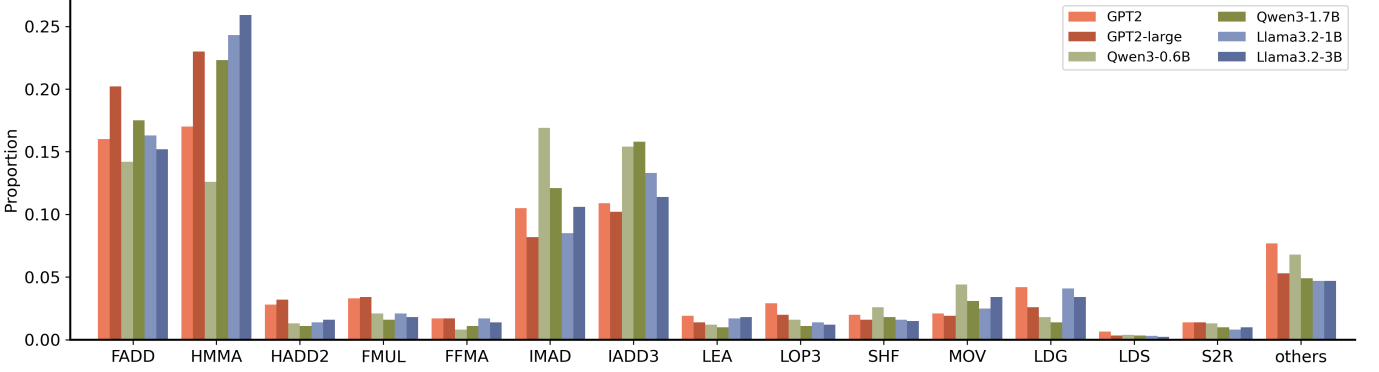


Fig. 6. Instructions Distribution of Different LLMs. Instructions that are fault-injectable but occur with negligible frequency (typically less than 0.01) are grouped into the Others category.

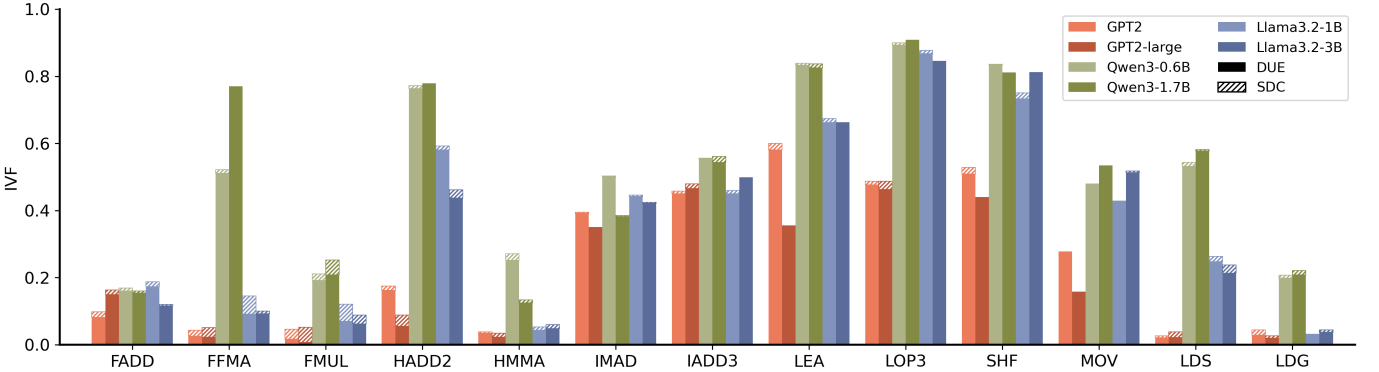


Fig. 7. IVF of different instructions. Solid color represents the portion contributed by DUE and diagonal line represents the portion contributed by SDC.

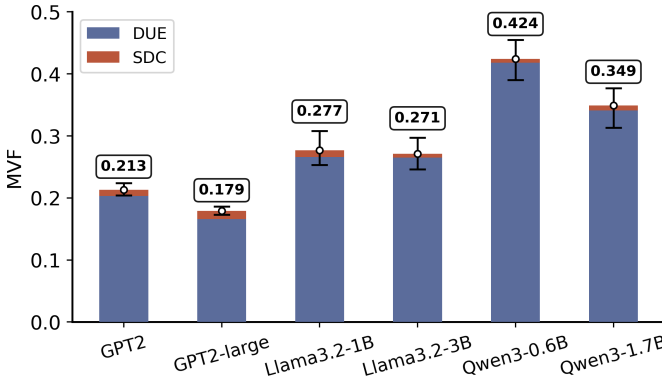


Fig. 8. Approximate Model Vulnerability Factor of different models. The error bars represent the standard deviation of the MVF over multiple experiments.

by instruction frequency. A small set of integer/address-related instructions (e.g., SHF, LOP3, LEA) are highly vulnerable and mainly lead to DUEs, whereas high-frequency floating-point compute instructions (e.g., FADD, HMMA) are relatively robust but still account for the majority of SDCs. At the same time, the IVF of the same instruction type is largely consistent across different models/architectures, with only a few floating-point and memory-related instructions exhibiting pronounced model-specific differences.

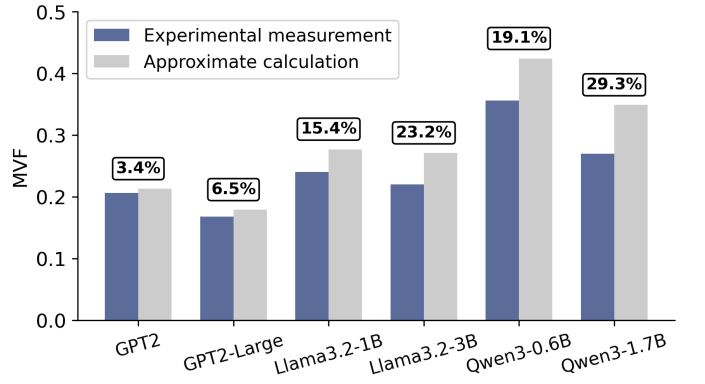


Fig. 9. Comparison of MVF obtained from experimental measurements and approximate computations, the numbers on top of the bars indicate the percentage difference.

2) *Calculate approximate MVF*: With this observation, we aim to further leverage IVF to calculate the overall vulnerability factor of the model, thereby enabling an efficient evaluation of the MVF. However, when applying traditional approaches—such as directly summing IVFs linearly or combining them using nonlinear independent-event probability models—the computed MVF deviates significantly from experimental measurements and fails to accurately capture the model’s overall vulnerability. To address this issue, We

propose a method of group-wise imputation and weighted aggregation approximation to calculate the MVF: using the proportion of each instruction type within the total instruction count as a weight, and performing a weighted accumulation of the IVFs to estimate the MVF, as shown in Algorithm 1. Since the number of instructions in some categories is very small, leading to prohibitively long evaluation times, we utilize an approximation calculation approach to determine the approximate lower bound and upper bound of the MVF, significantly reducing the evaluation time. Furthermore, we make the following assumption for this approximation: for instructions within the same group, the IVF of unmeasured instruction types is approximated by the average IVF of the measured instructions in that same group. The total sum of all instruction IVFs then approximates the model’s average MVF. The upper and lower bounds are approximated in a similar manner.

As shown in the experimental results in Figure 8, the MVF calculated using this proposed method closely matches the actual experimental data. This demonstrates that our method can effectively reflect the model’s overall vulnerability while simplifying the calculation process, offering a viable analytical means for subsequent fault-tolerance optimization.

3) *Compare with experimental results:* We quantify the overall vulnerability of each model through extensive fault-injection experiments, and then compare these results with model vulnerabilities approximated from instruction-level vulnerabilities, in order to evaluate the effectiveness of the approximation method. As shown in the Figure 9, the overall trends of model vulnerability obtained by the two approaches are highly consistent. Although the approximate computation introduces some numerical deviation, the error remains below 24% for all models except Qwen3-1.7B, whose deviation is 29.3%; for the GPT family, the deviation is even below 7%.

Our further analysis suggests that the main source of this deviation is that different instructions are typically not independent, but exhibit correlations and computational dependencies. As a result, approximating model-level vulnerability from instruction-level vulnerability tends to overestimate the overall vulnerability factor. Nevertheless, when focusing on the relative trends across models, this method still produces a relationship that is highly consistent with the ground-truth measurements, making it a practical and effective approximation for empirical evaluation.

B. Task Variations

Previous studies have shown that variations in input can lead to changes in model vulnerability. Although a model may appear highly reliable for certain inputs, there can still exist specific cases that significantly degrade its robustness. However, such observations are typically restricted to different samples within the same dataset. Motivated by this, we investigate whether LLMs exhibit different degrees of vulnerability under tasks of varying difficulty. To this end, we design a vulnerability analysis experiment for LLMs under different task difficulties, in order to characterize how model robustness changes across tasks. We select six datasets representing different difficulty levels—Lambada, Wikitext, PIQA, HellaSwag,

Algorithm 1 Approximate Computation of the MVF via Group-wise Imputation and Weighted Aggregation

Require: Instruction set I with instruction groups G ;

- 1: Measured instruction subset $M \subseteq I$, for which the instruction vulnerability factor v_i is experimentally obtained;
- 2: Unmeasured instruction subset $U = I \setminus M$, whose IVFs require estimation;
- 3: Function $g(i)$ mapping each instruction i to its group;
- 4: Proportion p_i of each instruction i in the target model, with $\sum_{i \in I} p_i = 1$.

Ensure: MVF bounds: V_{avg} , V_{min} , V_{max}

▷ Step 1: Derive group-wise IVF statistic

- 5: **for** each group $g \in G$ **do**
- 6: Identify measured and unmeasured instructions within group g :
- 7: $M_g = \{i \in M \mid g(i) = g\}$
- 8: $U_g = \{j \in U \mid g(j) = g\}$
- 9: Compute group-wise IVF statistics based on M_g :
- 10: $\mu_g = \frac{1}{|M_g|} \sum_{i \in M_g} v_i$ ▷ group-wise mean IVF
- 11: $\underline{v}_g = \min_{i \in M_g} v_i$ ▷ group-wise minimum IVF
- 12: $\bar{v}_g = \max_{i \in M_g} v_i$ ▷ group-wise maximum IVF
- 13: **end for**

▷ Step 2: Impute IVF for unmeasured instructions

- 14: **for** each unmeasured instruction $j \in U$ **do**
- 15: Let $g_j = g(j)$ denote the group of instruction j .
- 16: Assign group-wise statistics as IVF estimates for j :
- 17: $v_j^{avg} = \mu_{g_j}$, $v_j^{min} = \underline{v}_{g_j}$, $v_j^{max} = \bar{v}_{g_j}$
- 18: **end for**

▷ Step 3: Compute MVF bounds via weighted aggregation over all instructions

- 19: $V_{avg} = \sum_{i \in M} p_i v_i + \sum_{j \in U} p_j v_j^{avg}$
- 20: $V_{min} = \sum_{i \in M} p_i v_i + \sum_{j \in U} p_j v_j^{min}$
- 21: $V_{max} = \sum_{i \in M} p_i v_i + \sum_{j \in U} p_j v_j^{max}$
- 22: **return** V_{avg} , V_{min} , V_{max}

GSM8K, and XSum—which cover a broad range of scenarios including text generation, mathematical and commonsense reasoning, and language modeling. The performance of these models on the six datasets is summarized in Table III, and the difficulty posed by each dataset to the models varies considerably.

For datasets evaluated by accuracy, we choose single samples that can be consistently inferred correctly under fault-free conditions as test cases, since our focus is on whether injected faults cause deviations from the correct outputs. For datasets evaluated by PPL or ROUGE-1, we instead use a single text passage for evaluation. Because NVBitFI requires the execution of thousands of CUDA kernels during LLM inference, the time overhead is extremely high. In our experiments, running XSum on just one text passage generated trillions of dynamic instructions, making full-dataset fault injection prohibitively

time-consuming. Furthermore, we assume that faults do not occur in the KV cache, ensuring that the inference processes of different samples remain independent. Under this setup, we conduct 24,000 fault injection trials for each model on an NVIDIA A100 GPU, with a total runtime of approximately 800 hours.

Our primary focus is the degree of performance degradation caused by faults. As illustrated in the Figure 10, the models exhibit comparable levels of degradation on Lambada, PIQA, Hellaswag, and GSM8K, whereas the degradation is more pronounced on Wikitext2 and XSum. Moreover, as the number of injected faults increases, the accuracy of all models shows a clear downward trend across all datasets, but the magnitude and shape of the degradation curves vary substantially. We conduct a comparative analysis from the following three perspectives:

1) *Differences across tasks:* Among the six tasks, GSM8K and Lambada exhibit relatively stronger robustness: even after eight rounds of fault injection, some models still maintain an accuracy of 40%–50%. In contrast, Wikitext and XSum suffer the steepest declines. For example, GPT2 on Wikitext displays an almost cliff-like drop, with accuracy plunging from 68.6% to below 10%. This suggests that tasks centered on language modeling and long-text generation are more vulnerable to perturbations, whereas reasoning-oriented (GSM8K) and cloze-style (Lambada) tasks are comparatively less sensitive.

2) *Overall performance across models:* In terms of architecture, the GPT family consistently demonstrates stronger robustness than the Llama and Qwen family. For instance, on PIQA, GPT2-large still retains about 36.4% accuracy after eight rounds of fault injection, whereas Llama3.2-1B has already dropped to 25.0%. Similarly, GPT2 shows a slower degradation curve on Lambada and GSM8K. In contrast, the Qwen models exhibit moderate behavior: although their initial accuracy is relatively high, they degrade more rapidly under fault perturbations, especially on Wikitext and XSum.

3) *Impact of parameter scaling within the same architecture:* To examine how parameter scaling influences multi-task reliability under fault scenarios, we conduct experiments whose results are summarized in Table II. Enlarging parameter size induces pronounced task- and architecture-dependent effects on fault robustness. For natural language understanding tasks (Lambada, PIQA), Llama3.2 exhibits improved reliability with larger parameter counts, whereas GPT2 and Qwen3 suffer accuracy degradation. On XSum summarization, GPT2 and Qwen3 become more robust, while on WikiText-2 language modeling, GPT2 and Llama3.2 show enhanced reliability, underscoring architectural sensitivity to task type. For more challenging reasoning benchmarks (Hellaswag, GSM8K), most models exhibit reduced accuracy after scaling (except Qwen on Hellaswag), suggesting that parameter growth alone is insufficient to ensure fault robustness. Comparing different scales within the same architecture further reveals that, although larger models generally achieve higher fault-free performance, they degrade more rapidly under fault injection. For instance, GPT2-large surpasses GPT2 in nominal conditions but deteriorates faster under faults; similarly, Llama3.2-3B attains higher baseline accuracy than Llama3.2-

1B yet suffers more pronounced drops on GSM8K and XSum. These observations indicate that increased parameter capacity, while strengthening representational power, also introduces more complex computational pathways that can amplify error propagation and accelerate degradation. Thus, scaling up parameters can either enhance robustness or exacerbate vulnerability, contingent on task and architecture, highlighting the necessity of jointly considering task characteristics and fault-tolerance mechanisms when scaling models.

Insight #2: LLM fault robustness is strongly task- and architecture-dependent, and parameter scaling is not universally beneficial. Different tasks and architectures exhibit markedly different vulnerabilities under faults, and simply increasing model size—though improving fault-free accuracy—can either enhance robustness or accelerate degradation, depending on the task and architecture.

C. Bit Positions

To investigate the vulnerability characteristics of models at different bit positions, we conduct the following experiment: we modify the logic for computing the bit position in the fault injection function to fix a specific bit, and perform 500 fault injections for each bit position. To reduce the overall runtime, we inject faults every 4 bits from bit 0 to bit 28, and additionally include bits 30 and 31. The results are shown in Figure 11, which illustrates the impact of bit flips at different positions on system reliability, quantified in terms of both DUE and SDC. Several key observations can be made as follows:

1) *Low-order bits (bit 0-bit 12):* In the low-order bit range, the impact of faults is relatively small. The DUE probability mostly lies between 10% and 20%, with an average of 17.15%. The SDC rate remains below 1% for all models, and even below 0.5% for Llama3.2 and Qwen3, with the minimum as low as 0.15%. This indicates that bit flips in low-order bits are almost harmless and have limited impact on the overall model accuracy, suggesting that little fault-tolerance overhead is needed for these bits. However, bit 0 exhibits a higher DUE rate, with an average exceeding 26.4%, and thus requires special handling and additional protection.

2) *Middle-order bits (bit 16-bit 28):* In this range, the DUE probability increases on average by 5.34%, reaching 17%–33.4% overall. The effect is more pronounced in smaller models such as GPT2 and Qwen3-0.6B, where the average DUE probability on Qwen3-0.6B reaches 28.85%. In contrast, the SDC rate in this range remains between 0.3% and 1.15%, which represents no substantial increase compared with low-order bits. This implies that bit flips in middle-order bits are still unlikely to cause SDC. Therefore, the reliability threat posed by middle-order bit errors also lies primarily in DUE rather than accuracy degradation.

3) *High-order bits (bit 30-bit 31):* High-order bits (bit 30–31) are the most sensitive region to soft errors: the DUE probability remains in the 18%–30% range, and the SDC probability of bit 30 can reach 23.4% and 24.2% on GPT2 and Llama3.2, which are 26.52x and 95.8x higher than those of the corresponding low-order bits. This “bit-30 peak” stems from the IEEE single-precision format: bit 30 is the most

TABLE II
THE RELIABILITY CHANGES OF MODELS WITH THE SAME ARCHITECTURE AFTER INCREASING THE NUMBER OF PARAMETERS
(↑ REPRESENTS MORE RELIABILITY, ↓ REPRESENTS LESS RELIABILITY)

Model	Lambada	PIQA	Wikitext2	Hellaswag	gsm8k	Xsum
GPT2	↓	↓	↑	↓	↓	↑
Llama3.2	↑	↑	↑	↓	↓	↓
Qwen3	↓	↓	↓	↑	↓	↑

TABLE III
THE SCORING OF THE MODEL ON DIFFERENT DATASETS

Model	Lambada(ACC)	PIQA(ACC)	Hellaswag(ACC)	Wikitext2(PPL)	Xsum(ROUGE-1)	gsm8k(ACC)
GPT2	32.56	62.89	28.92	37.37	11.66	1.14
GPT2-large	47.66	70.35	36.40	22.61	11.80	1.52
Llama3.2-1B	62.22	74.32	47.68	11.56	12.74	6.60
Llama3.2-3B	70.04	76.71	55.21	9.26	12.86	25.85
Qwen3-0.6B	40.07	67.30	37.47	26.14	11.85	41.70
Qwen3-1.7B	50.30	72.09	46.14	21.04	13.06	69.14

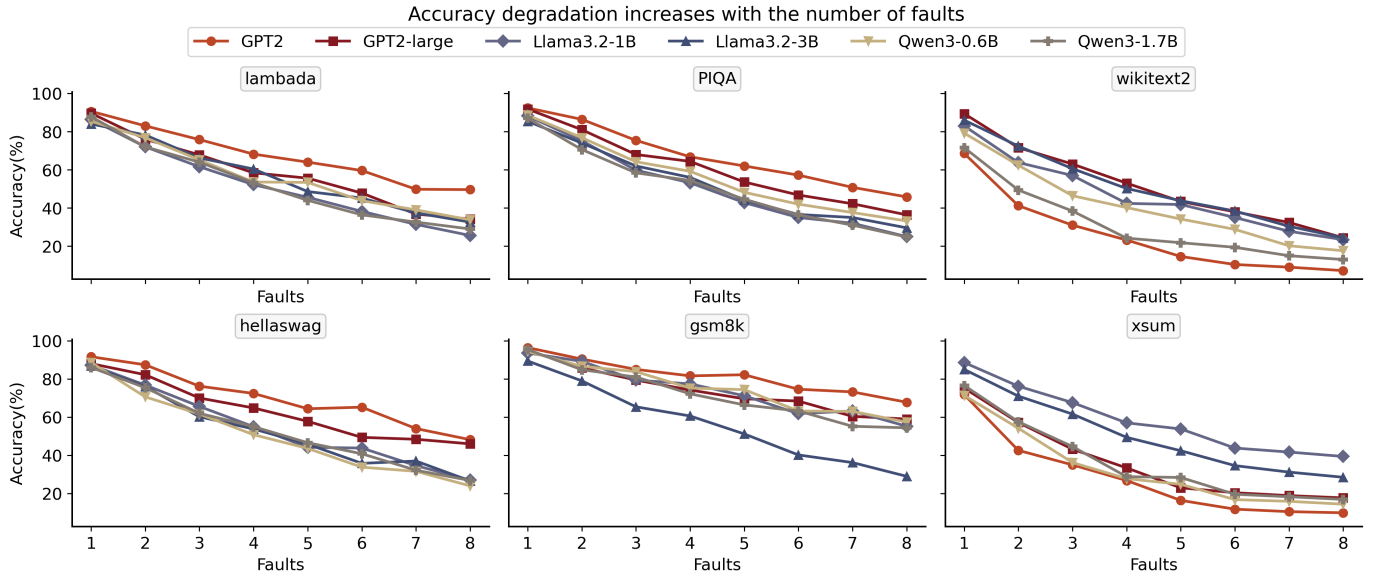


Fig. 10. The accuracy degradation of the model increases with the increasing number of faults during a single run. The accuracy here refers to the ratio of the number of correct inferences to the total number of experiments conducted.

significant bit of the exponent, so its flip induces cross-order-of-magnitude numerical deviations that are amplified during forward propagation and thus are very likely to evolve into SDCs. In contrast, the adjacent bit 31 is merely the sign bit; its flip only changes the sign and is often masked by subsequent nonlinear and normalization operations, making its contribution to SDCs far smaller than that of bit 30.

Insight #3: The impact of bit flips on LLM reliability differs markedly between SDC and DUE. SDC risk is highly bit-position-dependent: low-order bits are almost harmless, while high-order bits—especially the most significant exponent bit (bit 30)—are the primary source; in contrast, DUE is relatively uniform across bit positions. Thus, SDC mitigation should prioritize protecting high-order bits, whereas DUE reduction requires coverage of all bits; additionally, for some models (e.g., GPT2 and Qwen3), increasing model size can significantly reduce DUE rates.

D. Operator Types

We perform 5,000 fault injections for each model, which in total takes approximately 250 hours. By comparing the intermediate activations at each layer during inference with their corresponding golden values, we identify the modules where the injected faults take effect, and thereby derive the experimental results. Equation 1 shows the definition of operator vulnerability, where $V_{operator}$ denotes the vulnerability of a given operator, N_{error} denotes the number of erroneous model outputs, and $N_{inconsistent}$ denotes the number of cases where the operator output is inconsistent with the golden output. Since some faults may be masked during model inference, we only consider cases where the operator output exhibits a deviation.

$$V_{operator} = \frac{N_{error}}{N_{inconsistent}} \quad (1)$$

In our experiments, we inject faults into four main

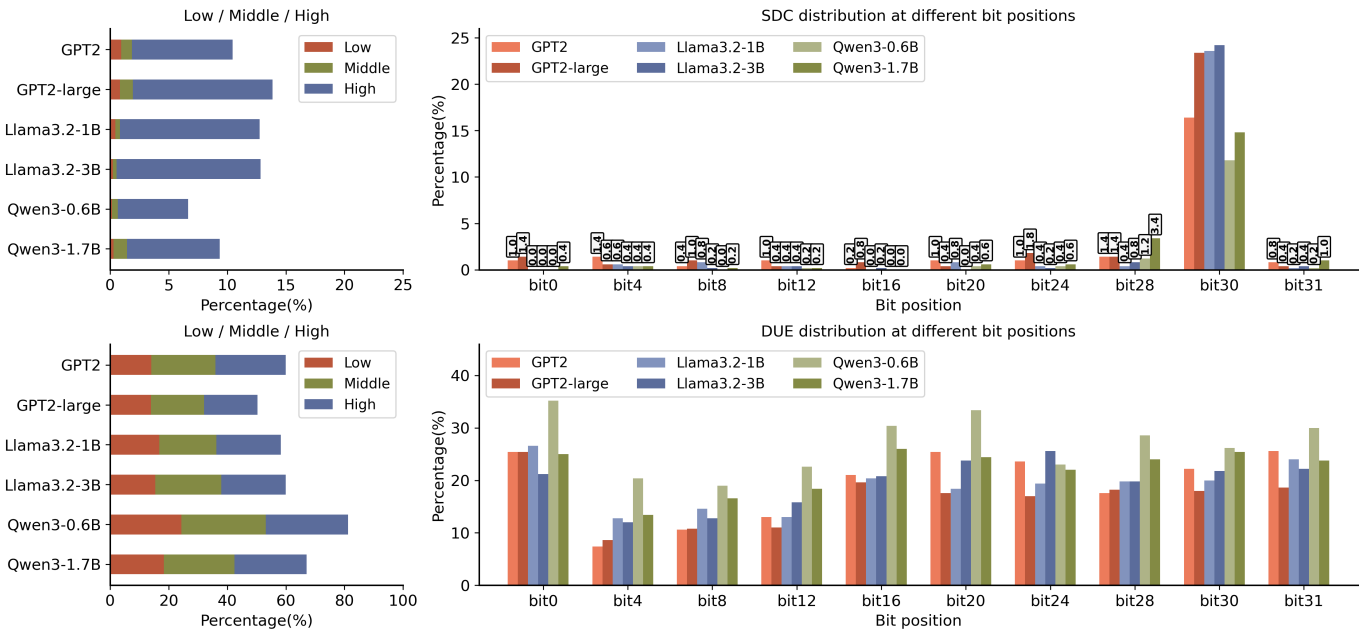


Fig. 11. The impact of bit-flip errors at different bit positions on system reliability in terms of DUE and SDC.

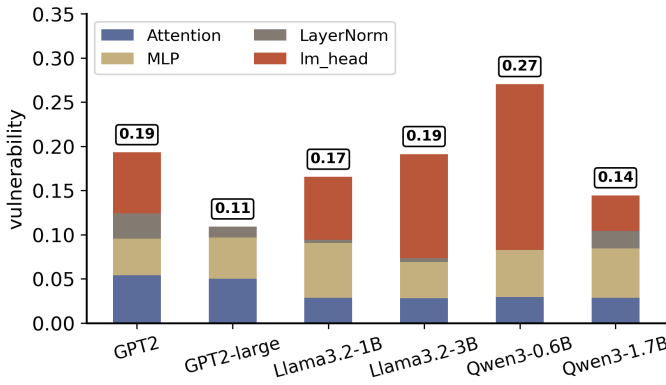


Fig. 12. Vulnerabilities of Different Operators in Multiple LLM Architectures.

operators—*Attention*, *MLP*, *LayerNorm*, and the *lm_head*—and quantify their vulnerabilities, as shown in Figure 12. Overall, these operators exhibit markedly different behaviors under soft errors. Among them, the *lm_head* consistently has the highest vulnerability across all models; in Qwen3-0.6B, its vulnerability even exceeds 0.18, making it the weakest component and indicating that the output layer plays a particularly critical role in the final prediction of LLMs. In contrast, *LayerNorm* shows the lowest vulnerability, generally below 0.02 for all models, suggesting that normalization operations possess strong fault tolerance and can be assigned a lower protection priority. *Attention* and *MLP* lie at an intermediate level (approximately 0.03–0.06): they exert a non-negligible influence on overall behavior, but are clearly less critical than the *lm_head*.

Regarding model scale, different model families exhibit distinct trends. In the GPT2 and Qwen3 families, larger-parameter models consistently show lower vulnerabilities across all op-

erators than their smaller counterparts, with reductions of 43.75% and 46.26%, respectively, particularly pronounced in the *lm_head*. This suggests that increasing parameter scale enhances the model’s error-absorption capability. In the Llama3.2 family, however, Llama3.2-3B exhibits an overall vulnerability 14.63% higher than Llama3.2-1B, again with a more evident increase in the *lm_head*, indicating that scaling up does not necessarily improve operator-level robustness.

Insight #4: Operator-level vulnerability to soft errors in LLMs is highly heterogeneous: the *lm_head* is consistently the most vulnerable operator, *LayerNorm* is the most robust, and *Attention/MLP* lie in between. Larger GPT2 and Qwen3 models reduce operator vulnerability, whereas Llama3.2 shows the opposite trend. Thus, fault tolerance should be selectively applied by operator and model size, prioritizing the *lm_head* (especially in smaller models) while relaxing protection for *LayerNorm* to reduce overhead.

E. Layer Variations

By conducting 5,000 fault injections on each model, we obtain the experimental results presented in Figure 13. The horizontal axis denotes the layer index of the stacked modules, while the vertical axis represents the vulnerability metric. Based on cross-model comparisons, we arrive at the following key observations:

First, within the GPT2 model family, GPT2-large shows a markedly higher overall error rate than GPT2, with vulnerable layers more widely distributed and a maximum error rate close to 0.3. This suggests that increasing parameter scale amplifies the susceptibility of certain layers to soft errors rather than mitigating it. The most vulnerable layers are mainly located at layers 0–2 and 13, 21, 23, and 27. In comparison, GPT2 has a lower overall error rate, but several layers (especially layers 0–1 and 9–10) still exhibit pronounced vulnerability.

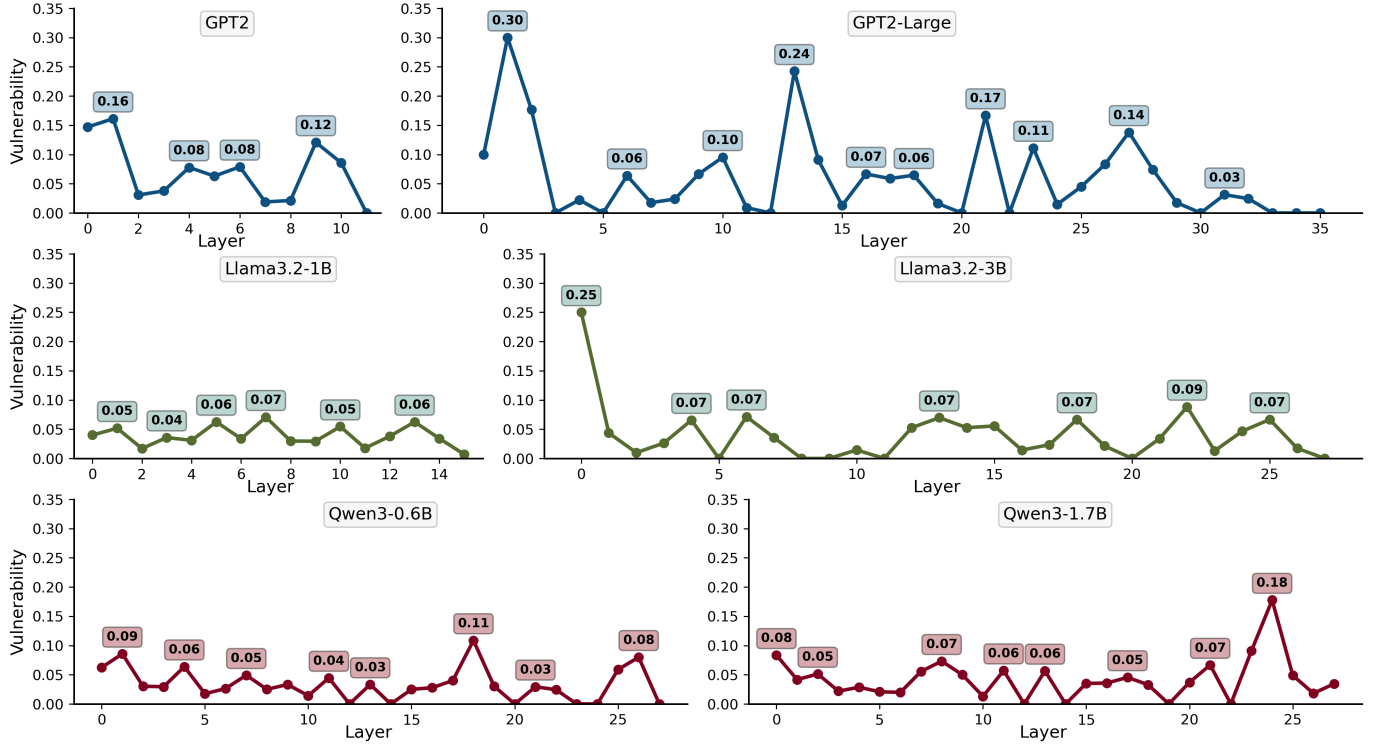


Fig. 13. Comparison of Error Rates in Different Layers, the horizontal axis represents different layers, and the vertical axis represents vulnerability.

Second, in the Llama3.2 family, Llama3.2-1B has the lowest overall error rate, with peaks below 0.1 and relatively small variation across layers. In Llama3.2-3B, however, the error rate of layer 0 approaches 0.3, indicating high vulnerability, while the error rates of the middle and deeper layers rapidly decrease and then stabilize. This pattern suggests that, as the parameter scale increases, the first layer of Llama3.2 models becomes significantly more sensitive to soft errors, whereas subsequent layers tend to be more robust. Third, in the Qwen3 family, overall error rates remain low, with most layers below 0.05. Nonetheless, several locally vulnerable layers still appear, such as layer 18 of Qwen3-0.6B and layer 24 of Qwen3-1.7B. This indicates that, although the Qwen3 family is generally more robust, a few individual layers can still act as potential high-risk points that warrant special attention in practical deployments.

We highlight an interesting phenomenon: as the model parameter scale increases, the overall shape of the layer-wise vulnerability distribution remains largely unchanged, yet the peak error rates rise significantly. This is mainly because larger models typically involve more attention heads or wider hidden dimensions, which intensify error propagation and accumulation in matrix operations, thereby leading to markedly higher local vulnerability peaks.

Insight #5: Layer-wise vulnerability to soft errors in LLMs exhibits pronounced local peaks rather than uniformly improved robustness with larger model scale. As model size increases, the overall shape of the layer-wise vulnerability distribution remains similar, while the peak error rates at specific layers grow significantly, indicating a shift from

broadly dispersed errors to concentration on a small set of critical layers.

V. CONCLUSION

We conduct a large-scale instruction-level fault injection study on GPU-based LLM inference systems, aiming to systematically characterize the manifestation and underlying causes of SDCs and DUEs during inference. Through extensive fault injection experiments and fine-grained analyses along multiple dimensions—including task difficulty, bit position, fault module, and network layer—we derive five key empirical observations regarding the fault behavior of LLM inference. Furthermore, we experimentally quantify the instruction vulnerability factor across different instruction types and leverage these measurements to approximate the overall instruction-level vulnerability of different LLMs. These results provide quantitative, instruction-level evidence for assessing and comparing the reliability of LLM inference systems.

REFERENCES

- [1] J. Achiam, S. Adler, S. Agarwal, L. Ahmad, I. Akkaya, F. L. Aleman, D. Almeida, J. Altenschmidt, S. Altman, S. Anadkat *et al.*, “Gpt-4 technical report,” *arXiv preprint arXiv:2303.08774*, 2023.
- [2] D. Guo, D. Yang, H. Zhang, J. Song, R. Zhang, R. Xu, Q. Zhu, S. Ma, P. Wang, X. Bi *et al.*, “Deepseek-r1: Incentivizing reasoning capability in llms via reinforcement learning,” *arXiv preprint arXiv:2501.12948*, 2025.
- [3] C. Kalra, F. Previlon, N. Rubin, and D. Kaeli, “Armorall: Compiler-based resilience targeting gpu applications,” *ACM Transactions on Architecture and Code Optimization (TACO)*, vol. 17, no. 2, pp. 1–24, 2020.
- [4] P. E. Dodd and L. W. Massengill, “Basic mechanisms and modeling of single-event upset in digital microelectronics,” *IEEE Transactions on nuclear Science*, vol. 50, no. 3, pp. 583–602, 2003.

[5] F. F. dos Santos, J. E. R. Condia, L. Carro, M. S. Reorda, and P. Rech, "Revealing gpus vulnerabilities by combining register-transfer and software-level fault injection," in *2021 51st Annual IEEE/IFIP International Conference on Dependable Systems and Networks (DSN)*. IEEE, 2021, pp. 292–304.

[6] G. Esposito, J.-D. Guerrero-Balaguera, J. E. R. Condia, and M. S. Reorda, "Evaluating different fault injection abstractions on the assessment of dnn sw hardening strategies," in *2024 IEEE 33rd Asian Test Symposium (ATS)*. IEEE, 2024, pp. 1–6.

[7] L. Yang, G. Papadimitriou, D. Sartatzakis, A. Jog, E. Smirni, and D. Gi-zopoulos, "Gpu reliability assessment: Insights across the abstraction layers," in *2024 IEEE International Conference on Cluster Computing (CLUSTER)*. IEEE, 2024, pp. 1–13.

[8] C. Bolchini, L. Cassano, A. Miele, A. Nazzari, and D. Passarello, "Analyzing the reliability of alternative convolution implementations for deep learning applications," in *2023 IEEE International Symposium on Defect and Fault Tolerance in VLSI and Nanotechnology Systems (DFT)*. IEEE, 2023, pp. 1–6.

[9] D. Sartatzakis, G. Papadimitriou, and D. Gi-zopoulos, "gpufi-4: A microarchitecture-level framework for assessing the cross-layer resilience of nvidia gpus," in *2022 IEEE International Symposium on Performance Analysis of Systems and Software (ISPASS)*. IEEE, 2022, pp. 35–45.

[10] J. D. Guerrero Balaguera, J. E. Rodriguez Condia, F. Fernandes Dos Santos, M. Sonza Reorda, and P. Rech, "Understanding the effects of permanent faults in gpu's parallelism management and control units," in *Proceedings of the International Conference for High Performance Computing, Networking, Storage and Analysis*, 2023, pp. 1–14.

[11] J. van Woudenberg, R. Velegalati, C.-B. Breunesse, and D. V. Riscure, "Improving cpu fault injection simulations: Insights from rtl to instruction-level models," in *2024 Workshop on Fault Detection and Tolerance in Cryptography (FDTC)*. IEEE, 2024, pp. 1–9.

[12] J. Tan, X. Li, A. Zhong, K. Yan, X. Wei, and G. Li, "Gerem: Fast and precise error resilience assessment for gpu microarchitectures," *IEEE transactions on parallel and distributed systems*, 2025.

[13] T. Tsai, S. K. S. Hari, M. Sullivan, O. Villa, and S. W. Keckler, "Nvbitfi: Dynamic fault injection for gpus," in *2021 51st Annual IEEE/IFIP International Conference on Dependable Systems and Networks (DSN)*. IEEE, 2021, pp. 284–291.

[14] O. Villa, M. Stephenson, D. Nellans, and S. W. Keckler, "Nvbit: A dynamic binary instrumentation framework for nvidia gpus," in *Proceedings of the 52nd Annual IEEE/ACM International Symposium on Microarchitecture*, 2019, pp. 372–383.

[15] J. Wei, A. Thomas, G. Li, and K. Pattabiraman, "Quantifying the accuracy of high-level fault injection techniques for hardware faults," in *2014 44th Annual IEEE/IFIP International Conference on Dependable Systems and Networks*. IEEE, 2014, pp. 375–382.

[16] Z. He, Y. Huang, H. Xu, D. Tao, and G. Li, "Demystifying and mitigating cross-layer deficiencies of soft error protection in instruction duplication," in *Proceedings of the International Conference for High Performance Computing, Networking, Storage and Analysis*, 2023, pp. 1–13.

[17] S. Wang, G. Zhang, J. Wei, Y. Wang, J. Wu, and Q. Luo, "Understanding silent data corruptions in a large production cpu population," in *Proceedings of the 29th Symposium on Operating Systems Principles*, 2023, pp. 216–230.

[18] H. Huang, C. Liu, X. Xue, B. Liu, H. Li, and X. Li, "Mrfi: An open-source multiresolution fault injection framework for neural network processing," *IEEE Transactions on Very Large Scale Integration (VLSI) Systems*, 2024.

[19] J. E. R. Condia, F. F. dos Santos, M. S. Reorda, and P. Rech, "Combining architectural simulation and software fault injection for a fast and accurate cnns reliability evaluation on gpus," in *2021 IEEE 39th VLSI Test Symposium (VTS)*. IEEE, 2021, pp. 1–7.

[20] A. Bakhoda, G. L. Yuan, W. W. Fung, H. Wong, and T. M. Aamodt, "Analyzing cuda workloads using a detailed gpu simulator," in *2009 IEEE international symposium on performance analysis of systems and software*. IEEE, 2009, pp. 163–174.

[21] C. Avalos Baddouh, M. Khairy, R. N. Green, M. Payer, and T. G. Rogers, "Principal kernel analysis: A tractable methodology to simulate scaled gpu workloads," in *MICRO-54: 54th Annual IEEE/ACM International Symposium on Microarchitecture*, 2021, pp. 724–737.

[22] B. Fang, K. Pattabiraman, M. Ripeanu, and S. Gurumurthi, "Gpu-qin: A methodology for evaluating the error resilience of gppu applications," in *2014 IEEE International Symposium on Performance Analysis of Systems and Software (ISPASS)*. IEEE, 2014, pp. 221–230.

[23] G. Li, K. Pattabiraman, C.-Y. Cher, and P. Bose, "Understanding error propagation in gppu applications," in *SC'16: Proceedings of the International Conference for High Performance Computing, Networking, Storage and Analysis*. IEEE, 2016, pp. 240–251.

[24] S. K. S. Hari, T. Tsai, M. Stephenson, S. W. Keckler, and J. Emer, "Sassifi: An architecture-level fault injection tool for gpu application resilience evaluation," in *2017 IEEE International Symposium on Performance Analysis of Systems and Software (ISPASS)*. IEEE, 2017, pp. 249–258.

[25] H. Huang, X. Xue, C. Liu, Y. Wang, T. Luo, L. Cheng, H. Li, and X. Li, "Statistical modeling of soft error influence on neural networks," *IEEE Transactions on Computer-Aided Design of Integrated Circuits and Systems*, vol. 42, no. 11, pp. 4152–4163, 2023.

[26] D. Xu, Z. Zhu, C. Liu, Y. Wang, S. Zhao, L. Zhang, H. Liang, H. Li, and K.-T. Cheng, "Reliability evaluation and analysis of fpga-based neural network acceleration system," *IEEE Transactions on Very Large Scale Integration (VLSI) Systems*, vol. 29, no. 3, pp. 472–484, 2021.

[27] X. Xue, C. Liu, Y. Wang, B. Yang, T. Luo, L. Zhang, H. Li, and X. Li, "Soft error reliability analysis of vision transformers," *IEEE Transactions on Very Large Scale Integration (VLSI) Systems*, vol. 31, no. 12, pp. 2126–2136, 2023.

[28] J.-D. Guerrero-Balaguera, R. L. Sierra, and M. S. Reorda, "Effective fault simulation of gpu's permanent faults for reliability estimation of cnns," in *2022 IEEE 28th International Symposium on On-Line Testing and Robust System Design (IOLTS)*. IEEE, 2022, pp. 1–6.

[29] G. Li, S. K. S. Hari, M. Sullivan, T. Tsai, K. Pattabiraman, J. Emer, and S. W. Keckler, "Understanding error propagation in deep learning neural network (dnn) accelerators and applications," in *Proceedings of the international conference for high performance computing, networking, storage and analysis*, 2017, pp. 1–12.

[30] Y. He, M. Hutton, S. Chan, R. De Gruijl, R. Govindaraju, N. Patil, and Y. Li, "Understanding and mitigating hardware failures in deep learning training systems," in *Proceedings of the 50th Annual International Symposium on Computer Architecture*, 2023, pp. 1–16.

[31] C. Liu, Z. Gao, S. Liu, X. Ning, H. Li, and X. Li, "Special session: Fault-tolerant deep learning: A hierarchical perspective," in *2022 IEEE 40th VLSI Test Symposium (VTS)*. IEEE, 2022, pp. 1–12.

[32] Y. He, P. Balaprakash, and Y. Li, "Fidelity: Efficient resilience analysis framework for deep learning accelerators," in *2020 53rd Annual IEEE/ACM International Symposium on Microarchitecture (MICRO)*. IEEE, 2020, pp. 270–281.

[33] Y.-S. Hsiao, Z. Wan, T. Jia, R. Ghosal, A. Mahmoud, A. Raychowdhury, D. Brooks, G.-Y. Wei, and V. J. Reddi, "Silent data corruption in robot operating system: A case for end-to-end system-level fault analysis using autonomous uavs," *IEEE Transactions on Computer-Aided Design of Integrated Circuits and Systems*, vol. 43, no. 4, pp. 1037–1050, 2023.

[34] X. Li, G. Yan, and C. Liu, *Built-in Fault-Tolerant Computing Paradigm for Resilient Large-Scale Chip Design: A Self-Test, Self-Diagnosis, and Self-Repair-Based Approach*. Springer Nature, 2023.

[35] D. Ma, F. Lin, A. Desmaison, J. Coburn, D. Moore, S. Sankar, and X. Jiao, "Dr. dna: Combating silent data corruptions in deep learning using distribution of neuron activations," in *Proceedings of the 29th ACM International Conference on Architectural Support for Programming Languages and Operating Systems, Volume 3*, 2024, pp. 239–252.

[36] L. Roquet, F. Fernandes dos Santos, P. Rech, M. Traiola, O. Sentieys, and A. Kritikakou, "Cross-layer reliability evaluation and efficient hardening of large vision transformers models," in *Proceedings of the 61st ACM/IEEE Design Automation Conference*, 2024, pp. 1–6.

[37] J. Ma, H. Pei, L. Lausen, and G. Karypis, "Understanding silent data corruption in llm training," *arXiv preprint arXiv:2502.12340*, 2025.

[38] K. Ma, C. Amarnath, and A. Chatterjee, "Error resilient transformers: A novel soft error vulnerability guided approach to error checking and suppression," in *2023 IEEE European Test Symposium (ETS)*. IEEE, 2023, pp. 1–6.

[39] T. Xie, J. Zhao, Z. Wan, Z. Zhang, Y. Wang, R. Wang, R. Huang, and M. Li, "Realm: Reliable and efficient large language model inference with statistical algorithm-based fault tolerance," *arXiv preprint arXiv:2503.24053*, 2025.

[40] U. K. Agarwal, A. Chan, and K. Pattabiraman, "Resilience assessment of large language models under transient hardware faults," in *2023 IEEE 34th International Symposium on Software Reliability Engineering (ISSRE)*. IEEE, 2023, pp. 659–670.

[41] A. Radford, J. Wu, R. Child, D. Luan, D. Amodei, and I. Sutskever, "Language models are unsupervised multitask learners," 2019.

[42] M. AI, "Llama 3.2 model card," https://github.com/meta-llama/llama-models/blob/main/models/llama3_2/MODEL_CARD.md, 2024.

- [43] Q. Team, “Qwen3 technical report,” 2025. [Online]. Available: <https://arxiv.org/abs/2505.09388>
- [44] D. Paperno, G. Kruszewski, A. Lazaridou, Q. N. Pham, R. Bernardi, S. Pezzelle, M. Baroni, G. Bolèda, and R. Fernández, “The lambada dataset: Word prediction requiring a broad discourse context,” *arXiv preprint arXiv:1606.06031*, 2016.
- [45] Y. Bisk, R. Zellers, J. Gao, Y. Choi *et al.*, “Piqa: Reasoning about physical commonsense in natural language,” in *Proceedings of the AAAI conference on artificial intelligence*, vol. 34, no. 05, 2020, pp. 7432–7439.
- [46] R. Zellers, A. Holtzman, Y. Bisk, A. Farhadi, and Y. Choi, “Hellaswag: Can a machine really finish your sentence?” *arXiv preprint arXiv:1905.07830*, 2019.
- [47] S. Merity, C. Xiong, J. Bradbury, and R. Socher, “Pointer sentinel mixture models,” *arXiv preprint arXiv:1609.07843*, 2016.
- [48] S. Narayan, S. B. Cohen, and M. Lapata, “Don’t give me the details, just the summary! topic-aware convolutional neural networks for extreme summarization,” *arXiv preprint arXiv:1808.08745*, 2018.
- [49] K. Cobbe, V. Kosaraju, M. Bavarian, M. Chen, H. Jun, L. Kaiser, M. Plappert, J. Tworek, J. Hilton, R. Nakano *et al.*, “Training verifiers to solve math word problems,” *arXiv preprint arXiv:2110.14168*, 2021.